Characterization of the Melt Quality and Impurity Content of an Lm25 Alloy

KATHARINA HABERL, PETER SCHUMACHER, GEORG GEIER, and BERNHARD STAUDER

The melt quality of an LM25 aluminum casting alloy has been examined using reduced pressure test (RPT) measurements, porous disc filtration analysis (PoDFA), and fatigue and tensile tests. The aim of this study was to determine the existing melt quality and thus to evaluate methods used with respect to monitoring and improving melt cleanliness. Special emphasis was given to the influence of oxides. It was found that the melt quality has varying degrees of effect on the tests used. The results indicate in particular that it was necessary to distinguish between "new" oxides (bifilms) and "hard" inclusions in the melt, as new oxides impact on porosity, whereas hard inclusions impact on ductility. Based on the results of this study, suggestions for the measurement of the melt quality have been proposed.

DOI: 10.1007/s11663-009-9282-7

I. INTRODUCTION

ALUMINUM has a high affinity for oxygen and as a consequence readily forms an oxide. If a molten aluminum surface reacts with atmospheric oxygen, an oxide film is created immediately. This film can take different morphologies, depending on the alloying elements of the melt and the contact time with the oxygen.[1] A film created on the melt surface cannot be dissolved in the liquid solution; it remains solid. The formation of bifilms has been extensively described by Campbell.[1] Essentially, surface turbulences are the only possibility to entrain folded films (bifilms) into the melt,[1] which subsequently lead to casting defects, *e.g.*, cracks or pores.[2,3] All oxides are created by the described entrainment mechanism.

Furthermore, the following two forms of inclusions can be distinguished[4]: new oxides (bifilms) and hard inclusions (old oxides, nitrides, carbides, *etc.*). New oxides are created during filling and casting, and their shape is two-dimensional. In contrast, hard inclusions are created before or during the melting. Their shape can be described as three-dimensional. It has been proposed that trapped atmosphere in the form of N_2 and O_2 can react with the bifilm, so that the reaction products fill the bifilm and a hard inclusion is formed in the end.[5,6] In addition, new bifilms can fold and ravel during bulk turbulences into a compact mass.[7] For the nucleation of hydrogen pores, bifilms (new oxides) are particularly relevant. Moreover, the influence of other hard inclusions in the melt has to be considered for mechanical properties.

Porosity has a negative influence on the casting part. It decreases the mechanical properties (fracture elongation, tensile strength, fatigue life) and hinders potential applications for the castings. Two extreme morphologies of porosity are gas-driven and shrinkage-driven porosity.[8] The formation of each one cannot be separated from the other as they are both caused by bifilms; hence, porosity is a mixture of both these features,[1,9] as shown in Figure 1. However, in the reduced pressure test (RPT) method, samples are well fed during solidification. Thus, the influence of shrinkage on porosity formation can be viewed as negligible (although this depends also on solidification morphology). For this reason, the RPT is an ideal measurement method for the determination of gas pores and a qualitative measurement for the gas content.

A qualitative trend between hydrogen content in the liquid and density of the RPT sample is apparent as long as sufficient nucleation sites exist (bifilms). At higher hydrogen concentrations in the liquid, a sufficient number of nuclei does not exist for a sufficient pore formation and growth of pores to obtain equilibrium so that large scatter of data becomes apparent. At lower hydrogen content in the liquid, nucleation sites have most often been depleted by, *e.g.*, impeller treatment, so that again pore formation is hindered and equilibration conditions are difficult to obtain.[10,11]

The measurement of the melt quality is not trivial, because new oxides are in at least one dimension very thin. Oxides are assumed to have a big influence on the formation of gas pores and, thus, quality. Most melt cleanliness assessments cannot measure bifilms in a

KATHARINA HABERL, Scientific Researcher, and PETER SCHUMACHER, Professor and Head of Department, are with the Chair of Casting Research, Metallurgy Department, University of Leoben, 8700 Leoben, Austria. Contact e-mail: katharina.haberl@unileoben.ac.at. PETER SCHUMACHER, Managing Director, and GEORG GEIER, Head of Tomography Group, are with the Austrian Foundry Research Institute, 8700, Leoben, Austria. BERNHARD STAUDER, Head of Process Development, is with NEMAK Linz GmbH, 4030 Linz, Austria.

This article is based on a presentation given in the "3rd Shape Casting Symposium," which occurred during the TMS Spring Meeting in San Francisco, CA, February 15–19, 2009, under the auspices of TMS, the TMS Light Metals Division, the TMS Solidification Committee, and the TMS Aluminum Processing Committee.

Article published online August 25, 2009.

satisfying way (*e.g.*, porous disc filtration analysis (PoDFA), pressure filtration melt cleanliness analyzer (PREFIL), ultrasonic measurements, liquid metal cleanliness analyzer (LiMCA)). Other recommended quality measurements like Dispinar's bifilm index[12,13] are notable but cover only pore-forming oxides and no hard inclusions, and it attaches much importance to the shape and length of the pores. The difficulty is to find a suitable method for detecting bifilms. Different impurities are measured by different measuring methods. Here, the melt quality is assessed by different techniques.

II. EXPERIMENTAL

A comprehensive study on the melt quality and the impurity content was performed. Special emphasis was given to bifilms and their effect on the melt quality. In all, 169 melt samples were collected.[14,15] For this publication, the secondary alloy LM25 was chosen because of many potential impurities contained within it.

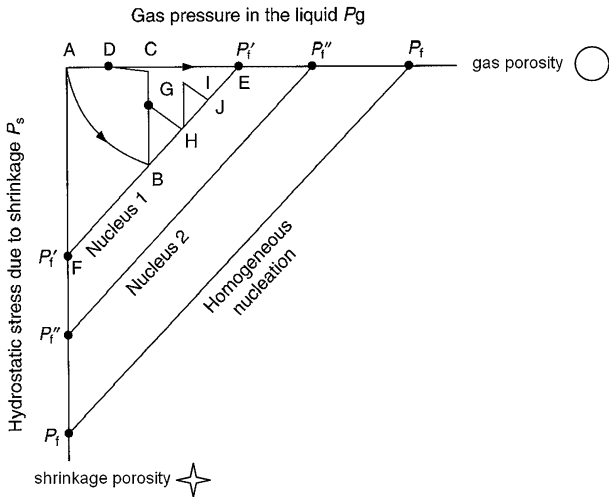

Fig. 1—Schematic diagram for the formation of porosity according to Campbell.[1]

The major alloying elements are Si (7 pct), Mg (0.23 pct to 0.45 pct), Cu (0.15 pct to 0.25 pct), Fe (<0.45 pct), Mn (0.15 pct to 0.35 pct), and Ti (0.08 pct to 0.16 pct). The exact composition was measured by spark analysis (SPECTROMAXx; Spectro Analytical Instruments GmbH, Kleve, Deutschland): Si (7.0 pct), Mg (0.4 pct), Cu (0.26 pct), Fe (0.35 pct), Mn (0.15 pct), and Ti (0.10 pct). The LM25 was melted in an induction furnace (medium-frequency coreless induction furnace, 1000 kW, 3.5 t; Otto Junker Group, Simmerath, Germany) and transported via a transport ladle (capacity 1 t) into the casting furnace (electric resistance furnace with silicon carbide crucible, 1 t; Carl Nolte GmbH, Greven, Germany). Samples were taken in the foundry from the melt in the transport ladle, from the casting furnace before rotary degassing, and from the casting furnace after rotary degassing for 15 minutes with N_2 at a melt temperature of 740 °C. The melt quality was determined using advanced RPT, PoDFA, tensile testing, and fatigue testing techniques.

A. *Reduced Pressure Test*

This test is used in conventional foundry handling for controlling the gas content of liquid metals. A sample was tested by solidifying a melt in a vacuum chamber under a standardized reduced pressure (80 mbar). Figure 2(a) shows the RPT apparatus (CG 16 K; BOC Edwards, West Sussex, U.K.) and Figure 2(b) RPT samples. The pores in the sample cause a change in density, which can be measured by the density index $DI = (\rho_{Atm} - \rho_{RPT}) \times 100/\rho_{Atm}$; ρ_{Atm} is the density of the sample solidified under atmospheric pressure and ρ_{RPT} is the density of the sample solidified under reduced pressure.

B. *Advanced RPT*

The RPT samples were examined by advanced RPT to detect pore distribution and geometry. The two methods of advanced RPT are metallographic image analysis of pores and porosity evaluation with computed tomography (CT).

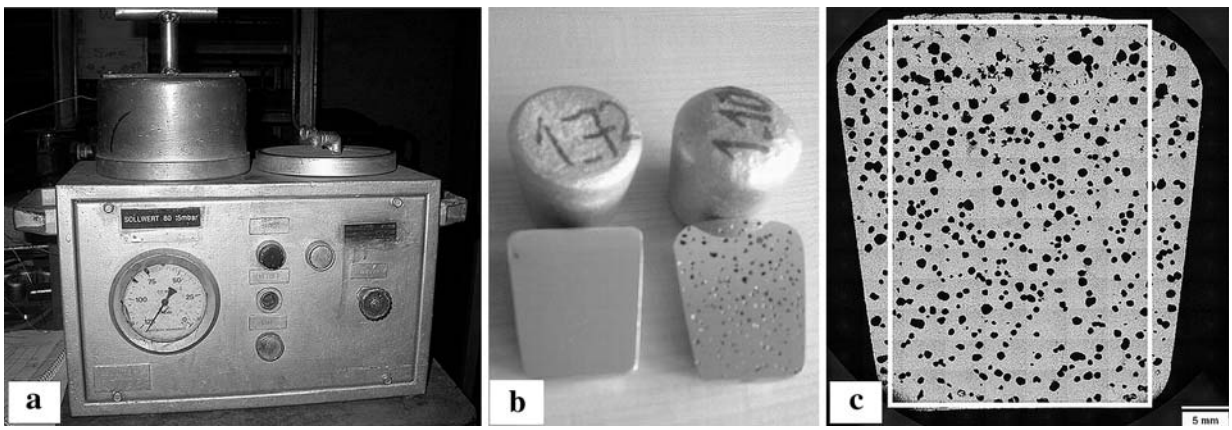

Fig. 2—(*a*) RPT apparatus, (*b*) RPT-samples (left: low gas content, right: high gas content), and (*c*) metallographic image analysis of the RPT-sample's cross section.

C. *Metallographic Image Analysis*

Pores in the cross sections were examined with a light microscope Nikon MM40; the number of pores per mm^2 was determined in a rectangular section (Figure 2(c)) by image analysis (NIS Elements Br 2.30, Nikon, San Diego, CA). For each condition, at least 4 RPT samples were taken and their cross sections were examined. The investigation of pores was performed in accordance with the Verein Deutscher Giessereifachleute (VDG) data sheet P201.[16]

In the current analysis, only the number density of highly active nucleation sites (bifilms) nucleating gas-driven pores in the initial stage of solidification under reduced pressure were measured. For this reason, the sink in volume (shrinkage pipe) was excluded. Therefore, the circularity must be at least 0.5 mm^2 and the pore size must be smaller than 7 mm^2. Furthermore, to avoid artifacts in the later parts of solidification caused by insufficient feeding, shrinkage-driven pores smaller than the dendrite arm spacings (DAS) (typically ~60 μm) were also excluded. The measurement results are given in pores per unit area. The concentration of pores in the cross section and the size distribution can thus be determined. Grinding and polishing may affect the porosity observed in the sample by stereography; as a consequence, three-dimensional CT was also employed.

D. *Computed Tomography*

Because of the geometrical and stereographical limitation of cross sections, it is not possible to measure the exact diameter of pores by metallography. It is necessary to conduct three-dimensional examination methods. With CT the pore diameter, the size and volume can be determined. CT delivers three-dimensional data sets that represent the local X-ray attenuation coefficient. To interpret these data sets according to pores, the interfaces between the pores and the surrounding material have to be defined exactly. Furthermore, pores and other inhomogeneities, especially shrinkage cavities, have to be distinguished. Advanced visualization techniques can give a near exact interface of the pores.[17]

Investigations of the RPT-samples have been made with a Phoenix X-ray v|tome|x-C CT system (Phoenix X-ray, Wunstorf, Germany). The experimental settings of the CT are described in Reference 17. An example of a comparison between the CT and metallographic evaluation is given in Figure 3. It shows a good correlation between the two investigative methods. The CT corroborates that the metallographic image analysis is a reliable way to detect the number of pores, as these do not show a convoluted morphology in RPT samples. Therefore, more investigations were done by image analysis of cross sections.

E. *PoDFA*

Undissolved hard or voluminous inclusions in the melt can be measured by filtration of the melt in PoDFA (ABB Hydro, Bonn, Germany). The area fraction inclusions are measured at a standard position above the filter (Figure 4). For each position (transport ladle and casting furnace before and after rotary degassing), at least five PoDFA samples were taken and their cross sections were examined. During filtration, a filter cake is built above the filter. This filter cake consists of particles from the melt, which can even be smaller than the pore diameter of the filter. However, participation of bifilms in the filter cake is limited because of their expected low stiffness. Furthermore, their detection is difficult because of their thin two-dimensional morphology. Within PoDFA, there is no specific category for bifilms. The typical spectrum of a PoDFA contains Al-oxide, Al-carbide, Ti-boride, Al-nitride, Mg-oxide, and spinel. However, coarse oxide films are usually detected with the PoDFA method.

The unit of measurement in PoDFA for melt impurity is in mm^2/kg given for different types of inclusions. In this article, the total accumulated values of inclusions

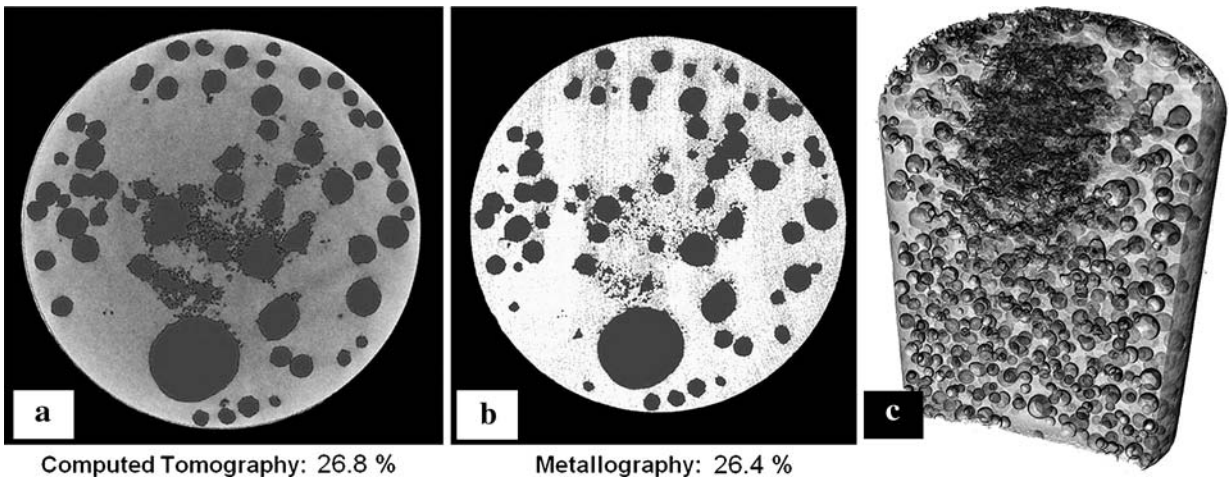

Fig. 3—(*a*) and (*b*) Porosity evaluation at corresponding positions: (*a*) CT analysis, (*b*) metallographic section, and (*c*) three-dimensional view of the CT sample (separating pores (light) and shrinkage cavities (dark)).

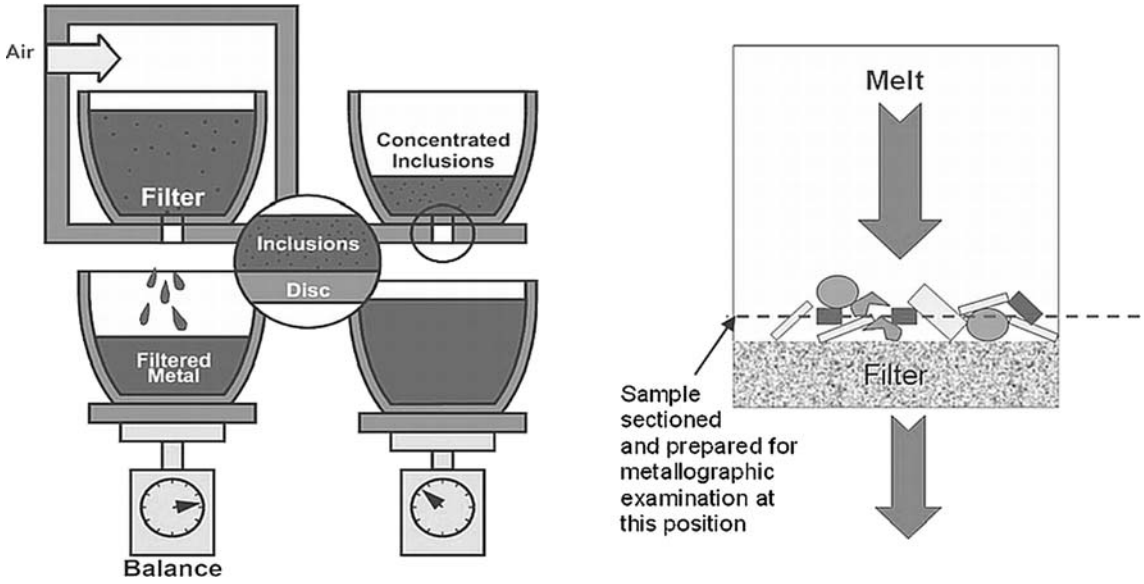

Fig. 4—Schematic view of the PoDFA apparatus and schematic illustration of filter cake with position for cross section.

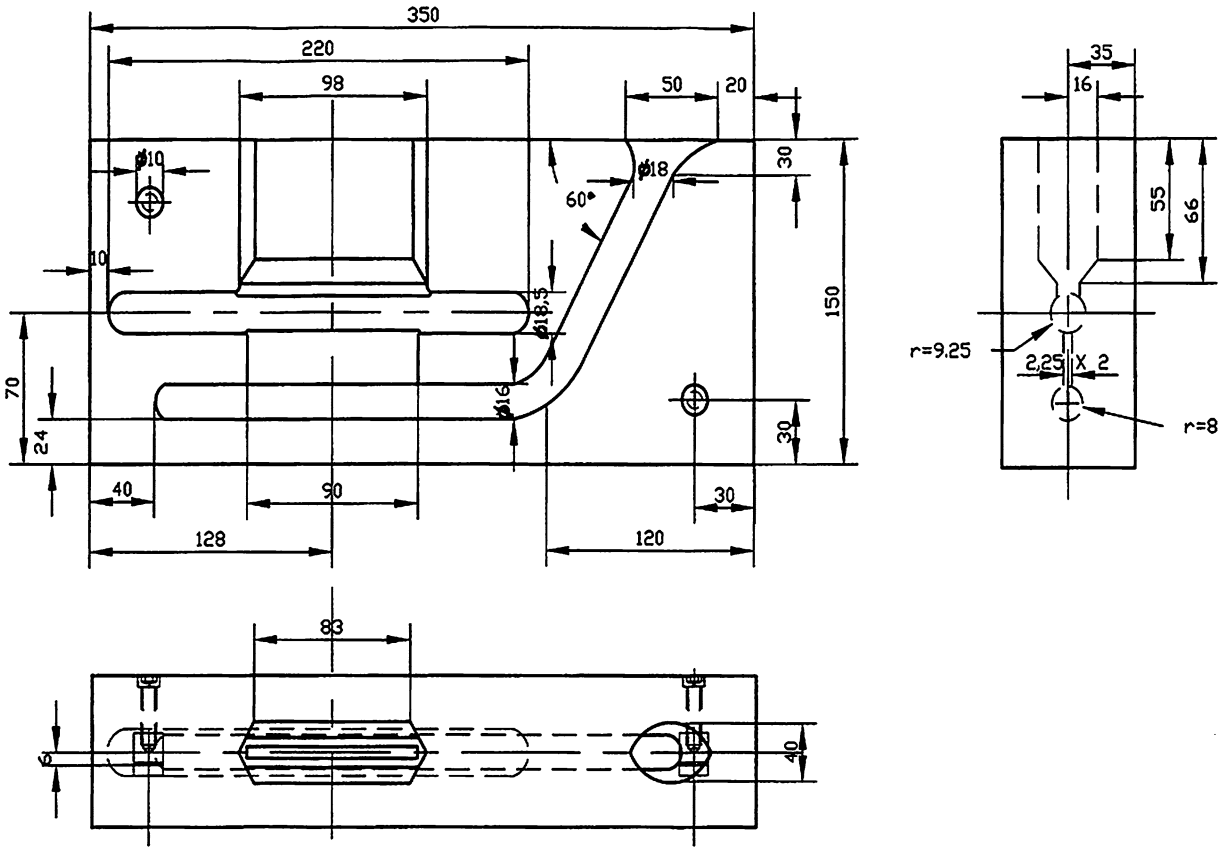

Fig. 5—Mold for manufacturing tensile and fatigue tests, including the gating system; dimensions are provided in millimeters.

are given. However, the results of the PoDFA give no information about the size of detected inclusions. Size is an important parameter for mechanical properties because large inclusions readily act as cracks. Inclusions are basically hard notches.

F. *Mechanical Testing*

Tensile and fatigue tests were manufactured in a steel mold (W300) with a gating system to produce cylindrical samples, the dimensions are shown in Figure 5. Typical

DAS were obtained in the range of 19 to 24 μm. The tests were performed on heat treated samples. In order not to obtain high fracture elongations as possible,[18] a special heat treatment was chosen. For the heat treatment, the samples were held at 200 and then 520 °C for a total of 2.5 hours, and then they were water quenched and artificial aged at 130 and then 200 °C for a total of 1 hour. The used heat treatment was chosen to sensitize the testing samples to obtain low fracture elongations, which thereby amplified the detection of defects. Before tensile testing, the tensile samples were machined from the casting in the mold into a testing section of Ø10 mm, 65 mm length with threaded ends (M16). The fatigue test samples were machined to Ø7 mm, 92 mm length with threaded ends (M16) and longitudinally mechanically polished.

For each sampling location, at least eight fatigue and tensile samples were performed. The tensile tests were conducted with a Zwick Roell Z050 (test standard EN 10002; Zwick Roell, Ulm, Germany) at Nemak Linz GmbH in Linz, Austria. For the interpretation of the tensile test, special emphasis is given to the fracture elongation A, as this is a sensitive parameter with high significance to melt purity. The fatigue tests were performed in compliance with accredited testing procedures (DIN 50100) on a Mikrotron 9201/129 (Russenberger Pruefmaschinen AG, Neuhausen am Rheinfall, Switzerland) resonant frequency machine at the Austrian Foundry Research Institute. For the fatigue testing, the stress ratio R was +0.05 and the upper stress σ_{max} was 160 MPa. A log-normal-distribution was performed for the interpretation of the measurements. The life-cycles before failure for a 90 pct survival probability were calculated using the program Visual-XSel 9.0 (CRGraph, München, Germany).

Fracture surfaces of tensile and fatigue tests were observed with a scanning electron microscope (SEM) Quanta 200 3D (FEI, Hillsboro, OR) with dual beam with an acceleration voltage of 20 kV. For element analysis, energy dispersive X-rays (EDX; Oxford Instruments, Oxfordshire, UK) were available.

III. RESULTS AND DISCUSSION

A. *Density Index (DI)*

Figure 6 shows the results for the DI at different stages in the manufacturing process. The value of every stage is a mean value composed of at least six samples.

The DI decreases during the melt treatment process. At the transport ladle, the DI is 10.8 and at the casting furnace before rotary degassing it is 9.2. Natural degassing in an atmosphere with lower H_2 pressure facilitates this observation, which should be more pronounced with longer times. In the casting furnace after rotary degassing, the DI decreases to a value of 0.8 as a result of the rotary degassing with N_2. Large scatter is observed for the high DI values in the transport ladle and at the casting furnace before rotary degassing. This scatter has also been reported in the literature.[10,14] After degassing, the scatter is significantly reduced.

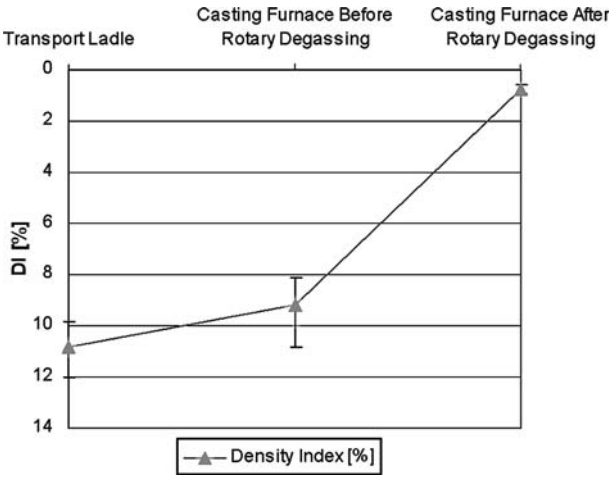

Fig. 6—Trend lines for the DI at different stages in the manufacturing process.

Usually a sufficient DI of melt chosen in industry is about 1. A DI of 1 corresponds closely with a hydrogen content of 0.1 mL/100 g at foundry conditions. Dasgupta *et al.*[19] reported a linear connection between the measured density of the RPT-sample and the hydrogen content measured with an Alscan sensor only at high hydrogen contents. Independent measurements with a hydrogen analyzer with an electrochemical sensor confirm this tendency to a certain extend.[14] Several papers[10,11,20,21] claim a qualitative (but not a quantitative) relation between the density of the RPT-samples and the hydrogen content rather melt cleanliness under certain conditions (*e.g.*, constant volume of the RPT-sample[10,20] and previous filtering of the melt[21]), and they acknowledge bifilms and other nucleation relevant inclusions a strong impact on DI. However, measured hydrogen content and DI do not show a linear dependence at low hydrogen concentrations.[10,14,15,19]

B. *PoDFA*

Figure 7 shows the results for PoDFA at different stages in the manufacturing process. The value of every stage is a mean value composed of at least five samples.

A significant influence of sedimented sump after decanting of the transport ladle can be observed. In the transport ladle, the value is 0.6 mm^2/kg. After the decanting in the casting furnace, the value before rotary degassing is 1.1 mm^2/kg because of the melt accumulation with hard inclusions (oxides and other carbides, nitrides, *etc.*). During degassing, impeller bubbles wet inclusions and float into the dross, whereas at longer holding times impurities sink to the bottom of the furnace. The value in the casting furnace after rotary degassing was 0.4 mm^2/kg.

The scatter in the experimental data in PoDFA is the largest in the casting furnace before rotary degassing, as the influence of the sump by unintentional stirring during decanting/filling of the furnace creates somewhat irregular inclusion patterns in the melt. The values for

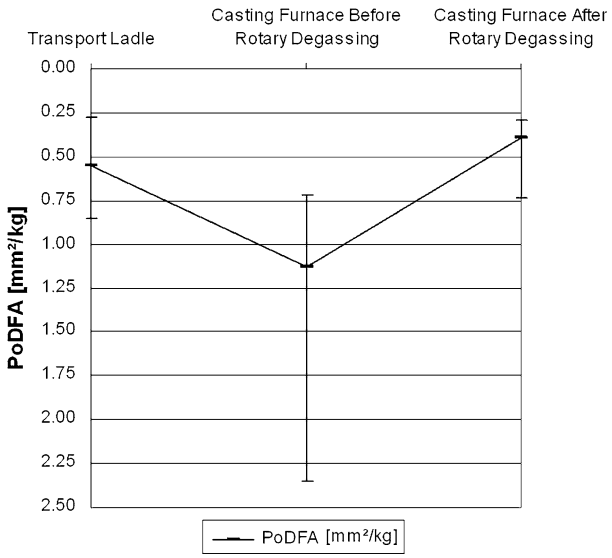

Fig. 7—Trend lines for PoDFA at different stages in the manufacturing process.

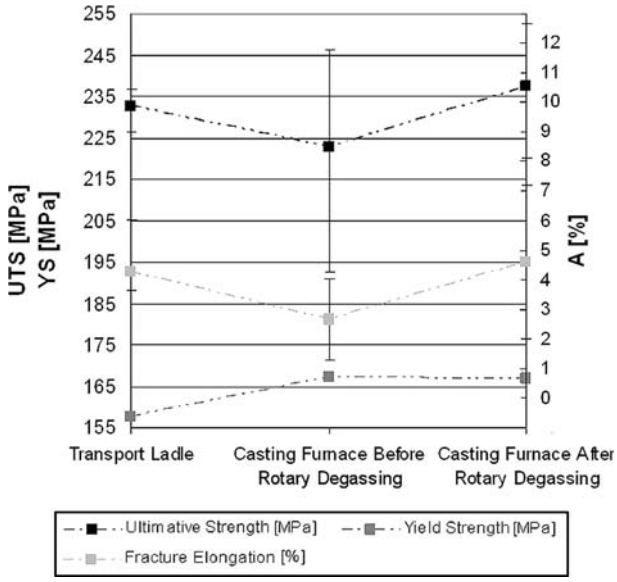

Fig. 8—Trend lines for A, UTS, and YS at different stages in the manufacturing process.

the transport ladle and the casting furnace after rotary degassing are in the order of ± 0.3 mm^2/kg.

C. *Tensile Properties*

Figure 8 shows the results of the tensile tests for fracture elongation A, ultimate tensile strength (UTS), and yield strength (YS) at different stages in the manufacturing process. The value of every stage is a mean value composed of at least eight samples. Although YS is of great significance for the design and performance of casting, at low levels of porosity, the YS is not affected greatly. Less then 1 MPa difference was found between the YS of 167 MPa before and after rotary degassing. Only the high gas content in the transport ladle reduced the YS to 157 MPa. A larger influence is found for UTS and fracture elongation.

At the tensile properties, the sedimented sump also had a significant influence. The fracture elongation of the transport ladle samples is 4.3 pct and the ultimate tensile strength 232.8 MPa, but the value for the casting furnace before rotary degassing reduces A to only 2.7 pct and UTS to 222.7 MPa. After the rotary degassing, impurities either are washed into the dross or sink to the bottom of the furnace. The fracture elongation A in the casting furnace after rotary degassing is 4.6 pct and UTS is 237.4 MPa. This implies that hard inclusions have a dominating influence on the tensile properties. Typical errors for the fracture elongation are ± 1.5 pct, and for the ultimate tensile stress, they are ± 20 MPa (transport ladle only ± 5 MPa). In Figure 9, the quality index diagram shows the correlation of A and UTS.

The tensile values are strongly influenced by the size of hard inclusions found in the fracture surface. Figure 10(a) shows such an inclusion at the fracture surface of a tensile test sample in SEM. Figure 10(b) is

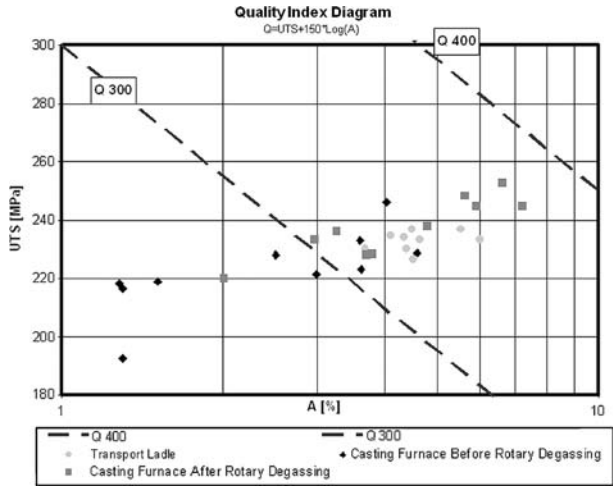

Fig. 9—Quality index diagram for different stages in the manufacturing process.

the corresponding oxygen elemental map. EDX from rough surfaces must be analyzed with care, but the map obtained appears to indicate the presence of oxides.

A qualitative correlation is found between PoDFA and tensile properties as a general trend: At low PoDFA values, high tensile properties values are observed. For these two parameters, the best melt quality is in the casting furnace after rotary degassing; good values are also achieved in the transport ladle, whereas the worst values are achieved in the casting furnace before rotary degassing.

D. *Pores/Area*

Figure 11 shows the results of the pores/area at different stages in the manufacturing process. The value

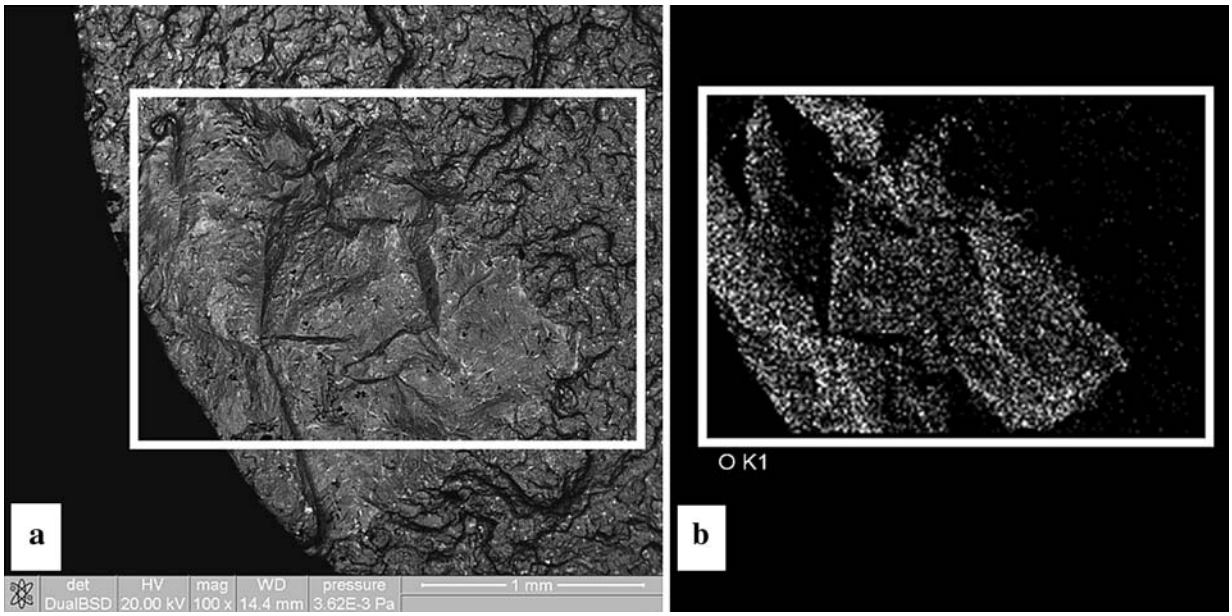

Fig. 10—(*a*) SEM: Typical fracture surface of a tensile test with inclusion (oxide) and (*b*) EDX: Distribution of the element oxygen in the framed area.

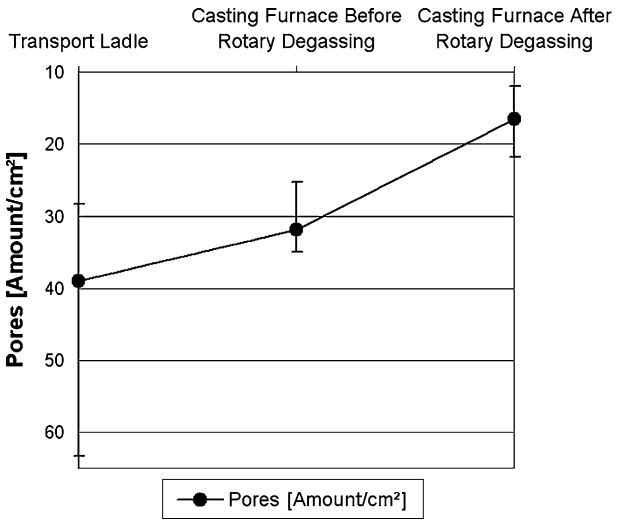

Fig. 11—Trend lines for pores/area at different stages in the manufacturing process.

of every stage is a mean value composed of at least four samples.

The amount of pores per area of the RPT sample shows an explicit increase of the melt quality during the treatment process. The amount of pores in the transport ladle is 39 pores/cm^2. At the casting furnace prior to rotary degassing, 32 pores/cm^2 and after the rotary degassing, only 17 pores/cm^2 are observed. The reason for this is the reduced amount of nucleation sites in the melt as a result of the rotary degassing. Again, the scatter is the highest for the transports ladle while in the casting furnace before and after rotary degassing the error is about ±5 pores/cm^2.

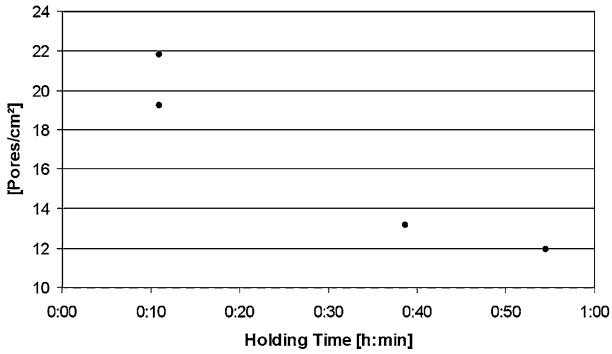

Fig. 12—The number of pores per area decrease at longer holding times in the casting furnace after rotary degassing.

The gas pores in the melt evolve from nuclei. Nucleation sites for pores in the RPT sample are assumed to be bifilms, which are activated by reduced pressure to form a pore. Thus, the number of bifilms or other inclusions that act as nuclei can be found by counting gas pores.[12–15,19] Interestingly, in holding experiments, the number of pores diminishes over time, which suggests that bifilms become inactive over time or are trapped as dross (Figure 12).

E. *Life Cycles*

Figure 13 shows the results of the life cycles at different stages in the manufacturing process. The single values of every stage are shown in the net diagrams in Figure 14. Similar to Tiryakioglu,[22] it was found that log-normal distribution fitted the data more convincingly.

The number of life cycles possible before failure increases during the melt treatment process. At the transport ladle, the life cycles with a survival probability of 90 pct are 120,000; at the casting furnace before rotary degassing, it increases to 140,000, and at the casting furnace after rotary degassing, the life cycles are 220,000. The reason for this is the decreasing amount of bifilms as oxides in the melt. Oxides as bifilms cause pores, and pores cause low cycles to fatigue.[23,24] Wang and colleagues[4,8] demonstrate that only the maximum defect size is crucial for life cycles. However, the number of pores becomes important in real components as the probability to have a defect in a critical location increases with number density.[14,15] Figure 15 shows such pores on the fracture surface of a fatigue test sample in the SEM.

A clear trend exists between the findings of the RPT and the fatigue tests for the current conditions (see Figures 11 and 13): At low values for pores/area, there are high values for life cycles. The best melt quality is achieved at the casting furnace after rotary degassing, and the worst quality is reached at the transport ladle. After rotary degassing, the gas content has been simultaneously lowered so that fewer and smaller pores were present.

IV. CONCLUSION

The melt quality and impurity content of the aluminum casting alloy LM25 (secondary alloy) were analyzed by various methods. Special emphasis was given to the influence of bifilms as nucleation sites for gas pores. The advanced RPT gives information about the number of nuclei for the formation of gas pores.

Figure 16 shows the combined results at different stages in the manufacturing process of the alloy LM25. The values were standardized, so that it is possible to visualize all measurement values on two axes: On the left side are the purity values (DI, pores/area, PoDFA) and on the right side are the mechanical values (A, life cycles). The values at the top of the diagram represent

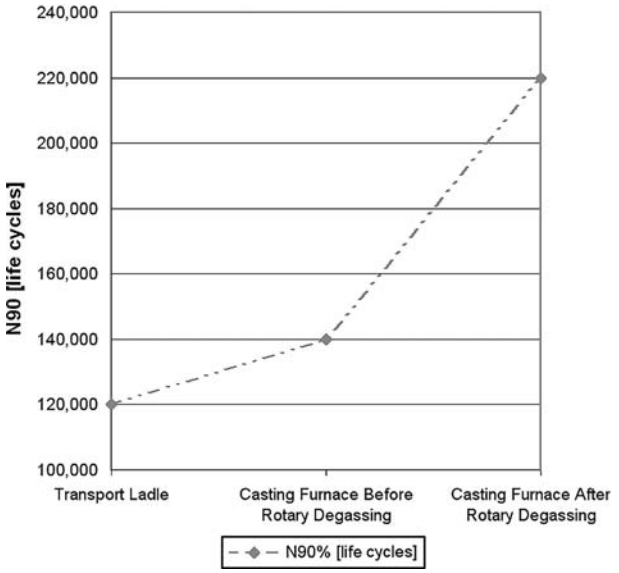

Fig. 13—Trend lines for life cycles at different stages in the manufacturing process.

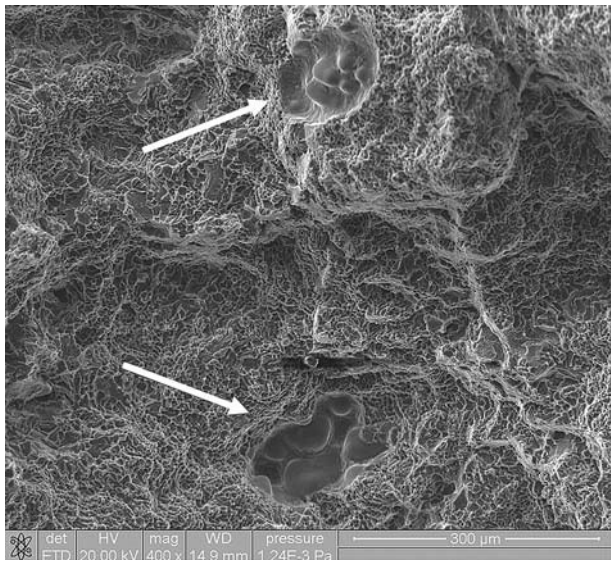

Fig. 15—SEM: Typical fracture surface of a fatigue test with porosities.

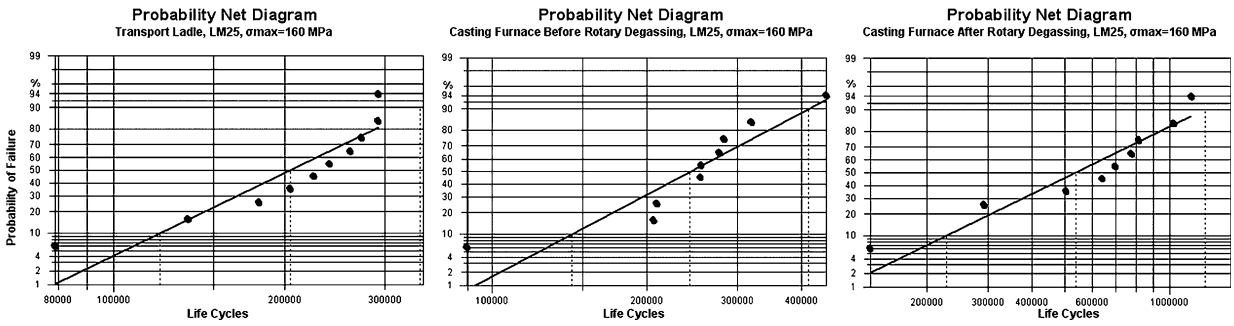

Fig. 14—Probability net diagram of fatigue tests at different stages in the manufacturing process, log-normal-distribution.

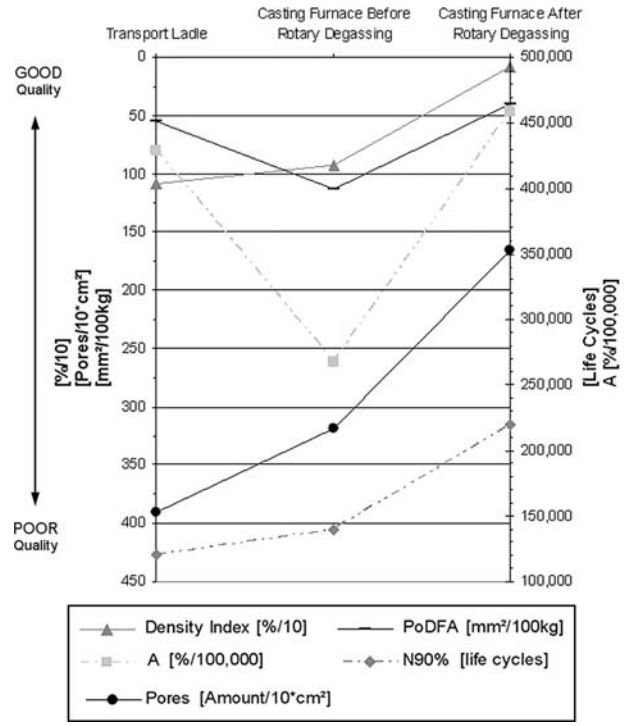

Fig. 16—The trend lines of the various measurements for the LM25 show an increase in the melt quality from the transport ladle and the casting furnace before rotary degassing to the casting furnace and after rotary degassing, with the exception of the fracture elongation and PoDFA. Here, the melt quality decreases in the casting furnace before rotary degassing during stirring of the sedimented sump by decanting of the transport ladle.

good melt quality, and the values at the bottom of the diagram confer to a poor melt quality.

The quality of the melt in the transport ladle and the casting furnace before rotary degassing is poor as expected and exhibits low life cycles, high amounts of pores in cross sections of the RPT-sample, high DI, and low fracture elongation (at the casting furnace before rotary degassing). The quality of the melt in the casting furnace after rotary degassing is improved, and it exhibits high life cycles, low amount of pores in the cross section of the RPT-sample, low DI, high fracture elongation, and a low value at PoDFA. A reason for this is the low gas content, the reduced amount of nucleation sites (especially bifilms), the resultant lower pore diameter, and presumably a more uniform pore distribution of smaller hydrogen pores in the melt. Special emphasis must be given to the casting furnace sedimented sump. The LM25 is a secondary alloy, and for this reason, the influence of the sedimented sump is more important. An accumulation and redistribution of particles from the sedimented sump occurs in the melt after each decanting of the transport ladle.

It is important to distinguish between old oxides and other hard inclusions or new oxides, such as bifilms. New oxides influence pore formation as bifilms, whereas the old oxides tend to act as hard inclusions and affect tensile properties.[4,14,15,25]

The life cycles are dominated by pores; therefore, they correlate well with the amount of pores and the DI of the RPT. Hard inclusions cannot be determined with the RPT; therefore, PoDFA or a similar method must be used. At low hydrogen contents, similar to that obtained in industry, the fracture elongation is ruled by hard inclusions. The tensile properties, in particular the fracture elongation, correlate well with the PoDFA results.

For the overall determination of the melt purity, the advanced RPT must be combined with PoDFA or similar methods.

ACKNOWLEDGMENTS

The practical measurements were performed at Nemak Linz/Austria, and the authors gratefully acknowledge Nemak Linz for their support, guidance, and excellent collaboration. The authors also acknowledge the Austrian Foundry Research Institute Leoben/Austria and the Competence Centre for Virtual Reality and Visualization VRVis Vienna/Austria. Part of this work was supported by the Austrian Research Promotion Agency.

REFERENCES

1. J. Campbell: *Castings,* Butterworth-Heinemann, Oxford, UK, 2003, pp. 12, 17, 65, 225.
2. E. Brunnhuber: *Giesserei Lexikon*, Schiele & Schön, Berlin, Germany, 1994, p. 864.
3. W. Hufnagel: *Aluminium-Taschenbuch*, Aluminium-Verlag GmbH, Düsseldorf, Germany, 1983, p. 377.
4. Q.G. Wang, C.J. Davidson, J.R. Griffiths, and P.N. Crepeau: *Metall. Mater. Trans. B,* 2006, pp. 887–95.
5. C. Nyahumwa, N.R. Green, and J. Campbell: *Met. Mater. Trans. A*, 2001, vol. 32A, pp. 349–57.
6. W. Griffiths, R. Raiszadeh, and A. Omotunde: *Shape Casting: 2nd International Symposium*, TMS, Warrendale, PA, 2007, pp. 35–42.
7. J. Campbell: *Mater. Sci. Technol.*, 2006, vol. 22, pp. 127–45.
8. Q.G. Wang and P.E. Jones: *Metall. Mater. Trans. B*, 2007, vol. 38, pp. 615–21.
9. E.J. Whittenberger and R.N. Rhines: *Trans. AIME*, 1952, vol. 194, pp. 409–20.
10. W. LaOrchan, M.H. Mulazimoglu, X.-G. Cheng, and J.E. Gruzleski: *AFS Trans.*, 1995, vol. 277, pp. 565–74.
11. K.J. Brondyke and P.D. Hess: *Trans. Metal. Soc. AIME*, 1964, vol. 230, pp. 1542–46.
12. D. Dispinar and J. Campbell: *Int. J. Cast Metals Res.*, 2004, vol. 17, pp. 280–86.
13. D. Dispinar and J. Campbell: *Int. J. Cast Metals Res.*, 2004, vol. 17, pp. 287–94.
14. K. Haberl: Master's Thesis, University of Leoben, Leoben, Austria, 2007.
15. K. Haberl, P. Schumacher, and G. Geier: *Giesserei,* 2008, pp. 48–54.
16. VDG-data sheet P 201, *VDG Verein deutscher Gießereifachleute*, Duesseldorf, Germany, 2002, pp. 1–16.
17. G. Geier, J. Rosc, M. Hadwiger, L. Fritz, D. Habe, T. Pabel, and P. Schumacher: *Shape Casting: 3rd International Symposium*, TMS, Warrendale, PA, 2009, pp. 131–39.
18. M. Tiryakioglu, J. Campbell, and N.D. Alexopoulos: *Metall. Mater. Trans. A,* 2009, pp. 1000–07.
19. S. Dasgupta, L. Parmenter, D. Apelian, and F. Jensen: *Proc. 5th International Molten Aluminum Processing Conference,* AFS Des Plaines, IL, 1998, pp. 283–300.

20. H.V. Sulinski and S. Lipson, *AFS Trans.,* 1969, pp. 56–64.
21. E.L. Rooy and E.F. Fischer: *AFS Trans*., 1963, vol. 76, pp. 237–40.
22. M. Tiryakioglu: *Shape Casting, 3rd International Symposium*, TMS, Warrendale, PA, 2009, pp. 35–44.
23. R. Minichmayr and W. Eichlseder: *Gießerei,* 2003, 5(B), pp. 70–75.
24. H. Leitner, W. Eichlseder, and Ch. Fagschlunger: *Gießerei Praxis*, 2006, vol. 3, pp. 70–76.
25. G.E. Byczynski and J. Campbell: *Shape Casting: The John Campbell Symposium*, TMS, Warrendale, PA, 2005, pp. 235–44.